CHAPTER 6

MULTIMODAL APPLICATION OF MAGNETO-FLUORESCENT HYBRID NANOSYSTEM

MULTIMODAL APPLICATION OF MAGNETO-FLUORESCENT HYBRID NANOSYSTEM

6.1 Introduction

Imaging is the diagnostic technique for detection of abnormalities before the treatment of the disease. These diagnostic techniques help the medical practitioners to recognize the infected parts without any surgery. The commonly used techniques to diagnose cancer cells are X-Rays, CT scans, MRI scans and PET scans. All these imaging modalities have their advantages as well as disadvantages in terms of sensitivity, specificity, accuracy, radiation exposure, costs and image acquisition time. X-rays are used to visualize bones, tumors and other dense matter inside the body. Computer Tomography (CT) scan is a more sophisticated way of employing X-rays for diagnostic purpose. However, exposure to X-ray radiation is known to have a chance of cancer occurring in the future. In some cases, anesthesia is also required and the use of contrast agents (dye) can cause kidney diseases. PET scan uses radioactive positrons to detect metabolic and chemical activity in the body [1-6]. A PET imaging is more sensitive than CT and MRI in terms of scar tissue differentiation, which has very little metabolic activity. But the major drawback is a PET scan is its accessibility, radiation exposure, and low spatial resolution. In MRI scans, strong magnetic fields and radio waves are used to form a detailed 3-D view of the selected organs and tissues in our body. However, it is relatively difficult to differentiate a scar tissue from the tumor using an MRI scan. It cannot be used on a person who has some metal implants. Also taking contrast agent orally for scanning is very unpleasant. Sometimes tissue imaging through MRI scan is not as clear as that of CT image. Thus, it can be told that every imaging technique has its own advantages and limitations also. Hence, merging different imaging modalities like CT/MRI and PET/MRI are conceived to complement the strengths of both the techniques in a synergistic way [7-10].

Now, the development of combo scans like CT/MRI and PET/MRI are in the conceptual stage of research and development. In this regard, a magneto-fluorescent hybrid nanomaterial, which has integration of superparamagnetic or paramagnetic nanosystem

with a quantum dot, will be useful for dual imaging (magnetic and fluorescent) application. This integration of fluorescence imaging (FI) with MR imaging (MRI) will be of great value to humans and the development of innovative treatment strategies. An attempt has been made in this thesis to bring this novel concept into reality. In the present thesis, the primary objective was laid down to develop magneto-fluorescent multimodal hybrid nanosystems for dual imaging applications. In achieving the aforementioned goal, the pristine magnetic nanosystems and quantum dots were synthesized and optimized based on their physical properties. Finally, the multimodal applicability of the prepared hybrid nanosystems has been evaluated as potential MRI contrast agent as well as fluorescent imaging probe.

6.2 Multimodal Applications

In recent times, nanotechnology has emerged with tremendous potential and possibilities for its applications in the biomedical field. The new generation biomedical applications will be based on multimodal or multifunctional nanosystems [11, 12]. These nanosystems were developed by integration of more than one functional component in a template or through conjugation to make them superior as compared to the individual system. The multimodal biomedical imaging is conceptualized based on hybrid probes of magneto-fluorescent, T_1-T_2, multimetallic etc. [13-15]. As no single imaging modality can provide all necessary information in an imaging application, hence the concept of multimodal molecular imaging agents have been conceived. Considering the unique characteristics of magnetic nanoparticles and quantum dots; both system have been integrated for development of magneto-fluorescent hybrid nanomaterials, in the present study. Magnetic nanoparticles can serve as contrast agent for magnetic resonance imaging (MRI) technique whereas fluorescent nanoparticles are used in imaging as well as monitoring of disease sites.

6.2.1 Biocompatibility

Toxicity Assay- Resazurin Reduction Assay

To study the potential interference of magneto-fluorescent hybrid nanosystems on live cells, cytotoxicity study was carried out to know about its biocompatibility [16, 17]. For quantifying *in vitro* cell viability with different type of hybrid nanosystems, Resazurin

Reduction Assay or Alamar Blue (AB) toxicity assay was performed. The detailed procedure for toxicity characterizations was described in **Chapter-3**.

Briefly, Murine RAW 264.7 macrophage cell line was used for *in-vitro* toxicity test. The 100 µl of cell suspension containing $1x10^4$ cells were seeded to each well of 96 well plates, excluding the ýrst row. After that, the plate was incubated at 37 °C, in an atmosphere of 5 % CO_2 and 90 % relative humidity for 1 hour (h). After 1 hour, the test sample volume i.e., 0.1 mL, 0.075 mL, 0.05 mL and 0.025 mL (**table-6.1**) were added to the wells of 96 well plates in triplicate culture. The 96 well plates were then incubated for 24 hours at 37 °C in an atmosphere of 5 % CO_2 and 90 % relative humidity. The experiment was repeated three times.

Table 6.1 Dose dependent concentrations of hybrid nanosystems

Si. no.	Sample	Concentration (Stock)	Volume	Dose dependent concentration
1	FePt@CdTe	0.01545 mg / mL	0.1 mL	0.001545 mg
			0.075 mL	0.001158 mg
			0.05 mL	0.000772 mg
			0.025 mL	0.000386 mg
2	FePt@CdSe	0.01652 mg / mL	0.1 mL	0.001652 mg
			0.075 mL	0.001239 mg
			0.05 mL	0.000826 mg
			0.025 mL	0.000413 mg
3	FePt@CdS	0.01655 mg / mL	0.1 mL	0.001655 mg
			0.075 mL	0.001241 mg
			0.05 mL	0.000827 mg
			0.025 mL	0.000413 mg

Alamar Blue (AB) reagent (resazurin) was added at the end of the 24 hours incubation, to 96 well plate having cell growth. The 96 well plates was then incubated for 4 hours at 37 °C and reaffirmed for color change. The absorbance signal is monitored at 540 nm. Absorbance data was collected in SpectraMax Plus 384 microplate reader

(Molecular Devices, USA) at 540 nm. After calculation of mean and standard deviation (SD = ů) from the repeated experiments, the cell viability was calculated using following formula:

$$\text{Cell Viability (\%)} = \frac{(\text{mean absorbance value of experimental group})}{(\text{mean absorbance value of control group})} \times 100$$

Concentration of stock solution of FePt@CdTe, FePt@CdSe and FePt@CdS hybrid nanosystems were 0.01545, 0.01652 and 0.01655 mg/mL in the toxicity experiments. The details of concentration are expressed in **table 6.1.** The control contains media and cells only. The % cell viability of control is taken as reference for calculation of cell viability with hybrid nanosystems.

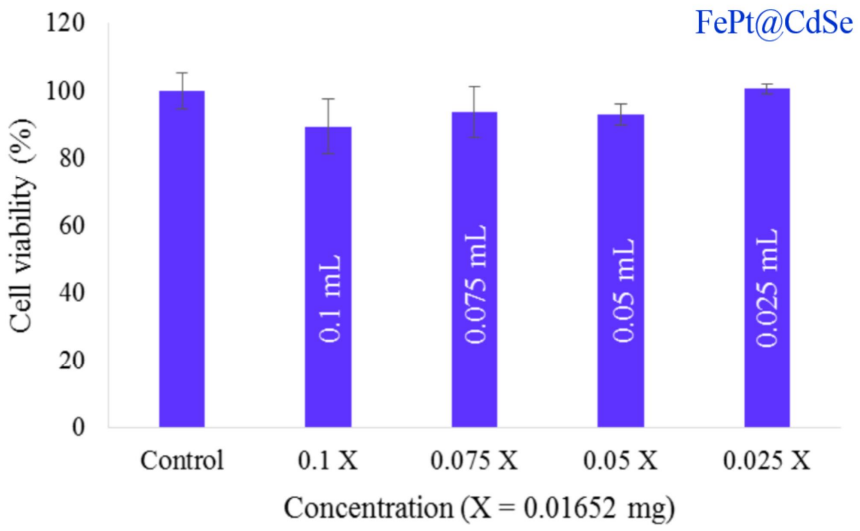

Figure 6.1 Viability of RAW 264.7 macrophage cell line compared to control indicated by AB assay when the cell was exposed to GSH capped hybrid FePt@CdTe nanosystem. The error bar was drawn using SD value

Figure 6.1, 6.2 and **6.3** exhibit the viability of RAW macrophage cell line with different doses of FePt@CdTe, FePt@CdSe and FePt@CdS hybrid nanosystems respectively.

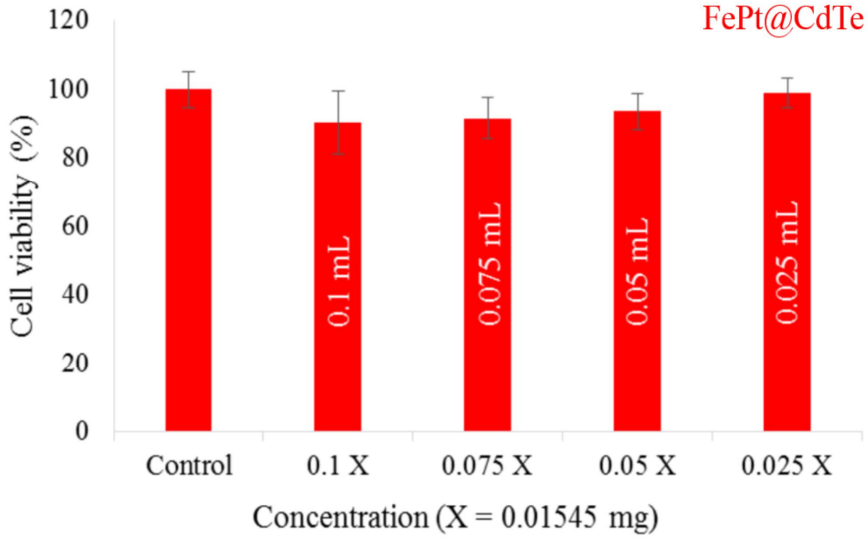

Figure 6.2 Viability of RAW 264.7 macrophage cell line compared to control indicated by AB assay when the cell was exposed to GSH capped hybrid FePt@CdSe nanosystem. The error bar was drawn using SD value

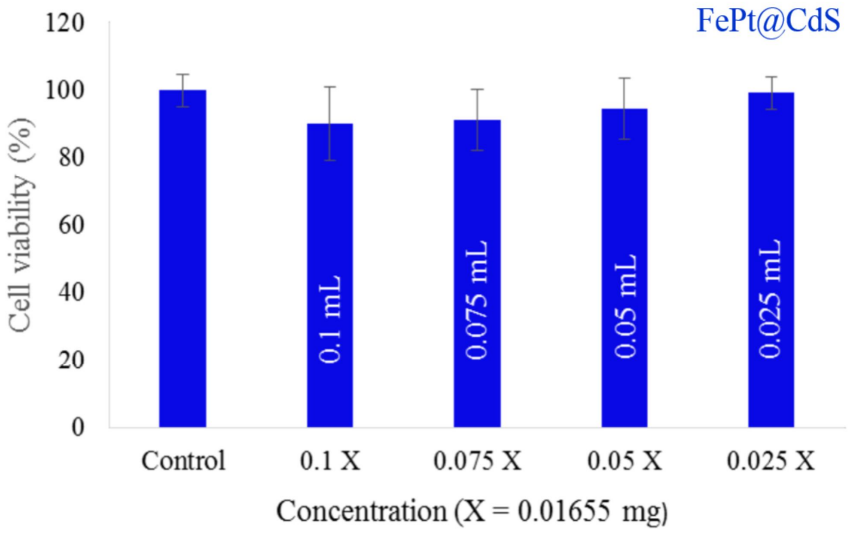

Figure 6.3 Viability of RAW 264.7 macrophage cell line compared to control indicated by AB assay when the cell was exposed to GSH capped hybrid FePt@CdS nanosystem. The error bar was drawn using SD value

In all the three different cases, % cell viability of RAW 264.7 macrophage cell line were not affected (< 80 %) by hybrid nanosystems even at 0.1 mL. It is also observed that

when the dose of hybrid nanosystem was decreased i.e. when the volume of test sample decreases from 0.1 to 0.025 mL, the viability of the cell increases. At the lowest dose, i.e. in 0.025 mL volume the viability is close to 100 % in all hybrid nanosystems.

6.2.2 Fluorescence imaging (FI) modality

The hydrophilic QDs or magneto-fluorescent hybrid nanosystems having bright fluorescence property and long-term stability make them suitable candidates for *in vivo* targeting and imaging [18-20]. In the previous section, the biocompatibility of hybrid nanosystems was discussed. The 96 well, which contain 0.05 mL volume of the test sample, was used for fluorescence imaging in each case. The preparation of slide for FI evaluation was done in a laminarflow cabinet. 20 µL sample taken from well contain 0.1 mL test sample onto the fresh slide and was covered by a coverslip. Images was taken by Leica trinocular inverted research microscope (Leica DMI 6000 B) with 63X oil-immersion objective lens under bright field and at an excitation wavelength of UV, blue and green light to examine its morphology and fluorescence property. After imaging, the cells were discarded using concentrated HNO_3 solution.

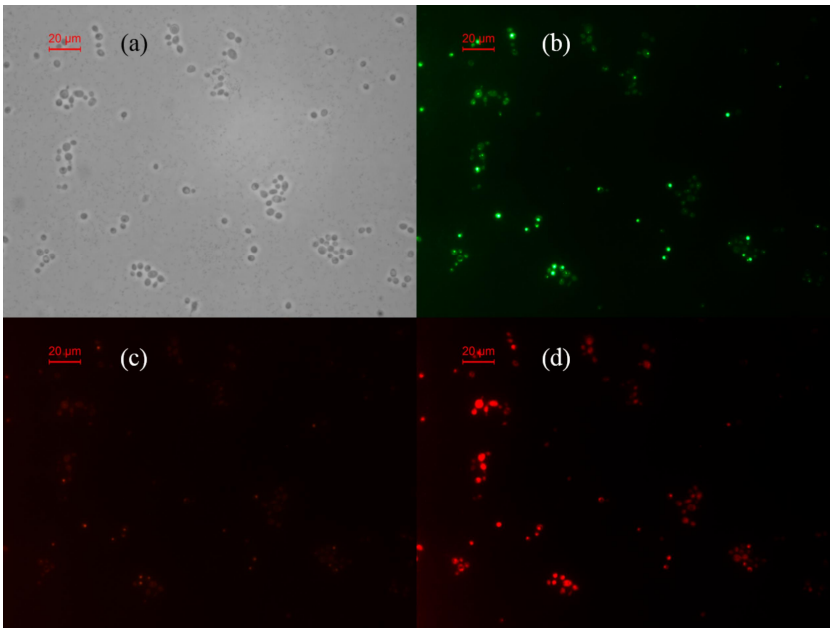

Figure 6.4 *In vitro* bright field and fluorescence images of GSH capped FePt@CdTe QDs in RAW macrophage cells. Images were taken by fluorescence microscope under (a) bright field and at an excitation wavelength of (b) UV (c) blue and (d) green light

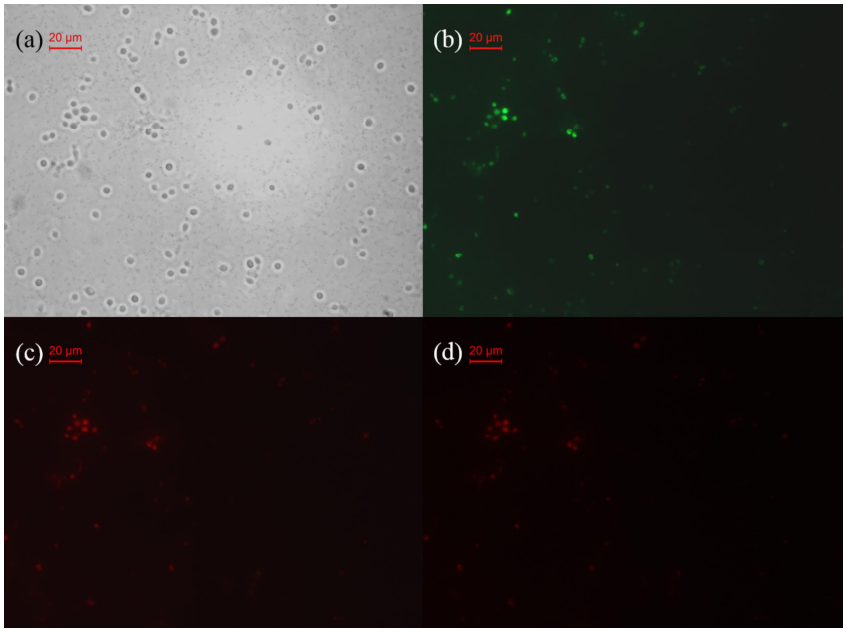

Figure 6.5 *In vitro* bright field and fluorescence images of GSH capped FePt@CdSe QDs in RAW 264.7 macrophage cells. Images were taken by fluorescence microscope under (a) bright field and at an excitation wavelength of (b) UV (c) blue and (d) green light

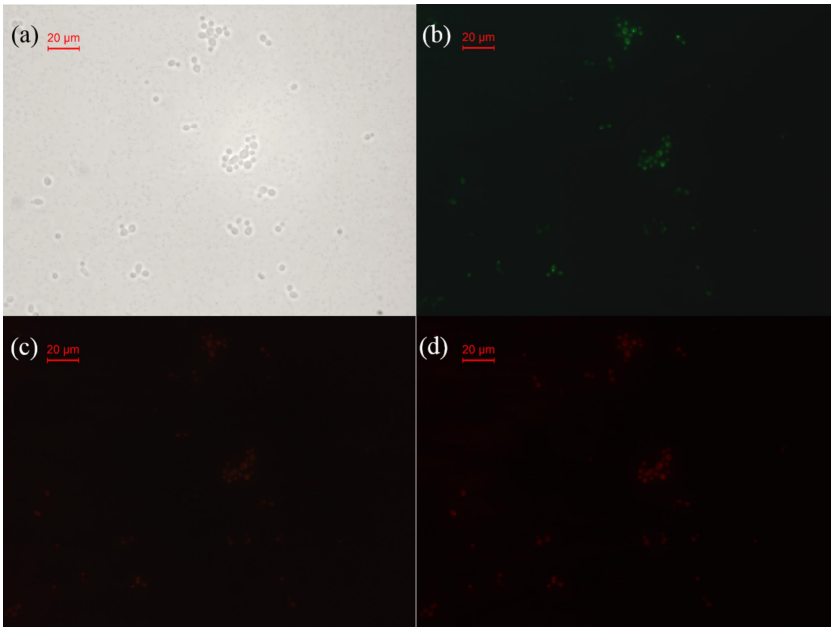

Figure 6.6 *In vitro* bright field and fluorescence images of GSH capped FePt@CdS QDs in RAW macrophage cells. Images were taken by fluorescence microscope under (a) bright field and at an excitation wavelength of (b) UV (c) blue and (d) green light

The fluorescence functionality of GSH capped magneto-fluorescent FePt@CdTe, FePt@CdSe, FePt@CdS hybrid nanosystems in RAW 264.7 macrophage cells are shown in **figure 6.4, 6.5** and **6.6** respectively. **Figure 4.18** has depicted bright field and fluorescence images of GSH capped CdS QDs. These cells contain fluorescent pink resorufin dye and produced a fluorescent signal at excitation wavelength 530-560 nm. In the imaging process, the samples were excited at UV, blue and green lights and their wavelengths (ৼ) correspond to 360, 450 and 530 nm respectively. The fluorescence image obtained using UV and blue excitation was exclusively due to quantum dots fluorescence whereas the green light excited fluorescence images have additional fluorescent contribution due to the dye. The bio-compatibility of the particles would be compromised due to UV excitation. The fluorescence property of dye has been explained in the **appendix-B.** It is seen that the intensity of fluorescence of FePt@CdTe and FePt@CdSe is superior to the FePt@CdS system. This can be correlated to the higher band gap of CdS QDs. Hence, it can be inferred that all the three hybrid core-shell nanosystems have the capability for targeting and biomedical fluorescence imaging.

6.2.3 MRI modality

The dipolar coupling among the magnetic moments of MNPs and magnetic moments of water protons cause effective spin dephasing and T_2 relaxation leading to decrease in signal intensity [21]. So, water protons play an important role to produce contrast difference. It is revealed from the earlier studies that the hydrophilic capping of MNPs produces more contrast with respect to hydrophobic coating in the same system [22]. The transverse relaxivity (r_2) of the MNPs (FePt-A) was discussed in **Section-3** (**figure 3.15**) of **chapter-3** [23]. In this chapter, the r_2 of magneto-fluorescent hybrid (FePt@CdTe, FePt@CdSe and FePt@CdS) nanosystems are discussed w.r.t. pristine FePt-A MNPs.

The transverse relaxation time measurement was carried out using a vertical wide bore (89 mm) 14.1 T magnet, equipped with 60 mm actively shielded gradient, interfaced with Avance II Microimager (Bruker Biospin, Germany). The transverse relaxivity (r_2) of the magneto-fluorescent hybrids (FePt@CdTe, FePt@CdSe and FePt@CdS) nanosystems were evaluated by measuring the transverse relaxation time (T_2) of water

in the presence of different quantity of test samples at 25 °C. The stock concentrations used for calculation of relaxivity of hybrid nanosystems are depicted in **table 6.1**.

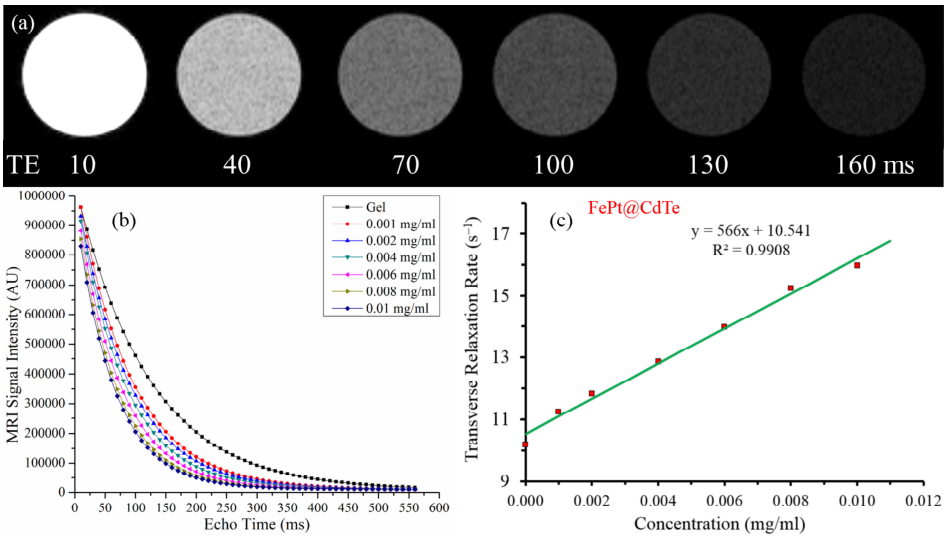

Figure 6.7 Transverse relaxivity characterization (a) typical MR images of microfuge tube containing FePt@CdTe (0.01 mg/ml in 0.5% agarose gel), (b) estimation of transverse relaxation time (T_2) of water and (c) transverse relaxivity of FePt@CdTe in 0.5% agarose gel

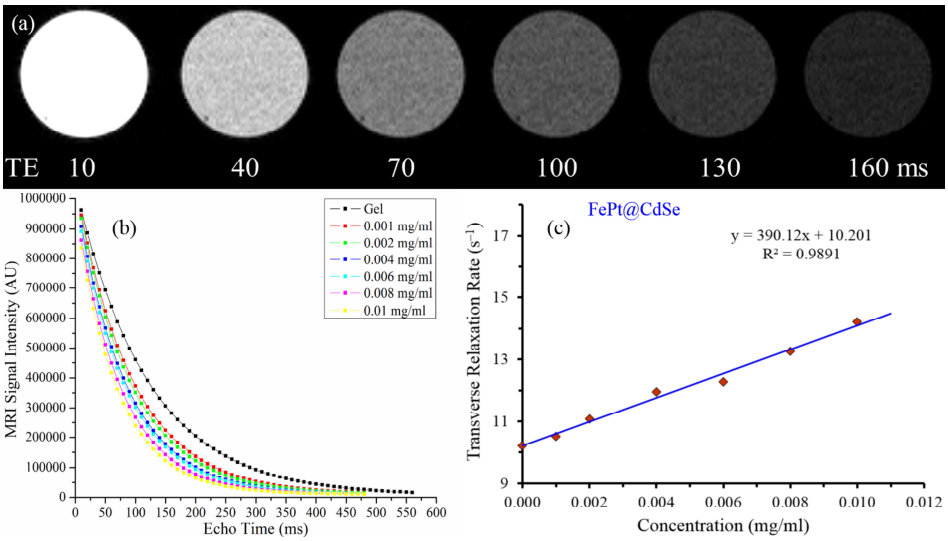

Figure 6.8 Transverse relaxivity characterization (a) typical MR images of microfuge tube containing FePt@CdSe (0.01 mg/ml in 0.5% agarose gel), (b) estimation of transverse relaxation time (T_2) of water and (c) transverse relaxivity of FePt@CdSe in 0.5% agarose gel

The effect of MNPs and magneto-fluorescent hybrid nanosystems on the spin-spin or transverse relaxation times (T_2) of water was studied. The transverse relaxivity measurement was carried out in 0.5% agarose solution. The axial magnetic resonance images (MRI) of microfuge tube containing MNPs and magneto-fluorescent hybrid nanosystems in Agarose Gel (0.5%) were obtained with varying echo times using multi-slice multi-echo (MSME) protocol depicted in **figure (a)** of **6.7, 6.8** and **6.9**. The water signal intensity was found to decrease with increasing echo time, analyzed using following mono-exponential function equation to derive T_2.

$$S_{TE} = S_{TE=0}\left(e^{-TE/T_2}\right)$$

Where, $S_{TE=0}$ is the signal of 0.5% agarose solution, TE is the echo time and T_2 is the transverse relaxation time. T_2 measurements of water were carried out with varying concentration of MNPs and magneto-fluorescent hybrid nanosystems depicted in the **figure (b)** of **6.7, 6.8** and **6.9**. The transverse relaxivity (r_2) measures the change in the spinï spin relaxation rate per unit concentration of test samples. The r_2 of MNPs and magneto-fluorescent hybrid nanosystems were estimated from the slope of relaxation rate ($R_2 = 1/T_2$) versus concentration graph.

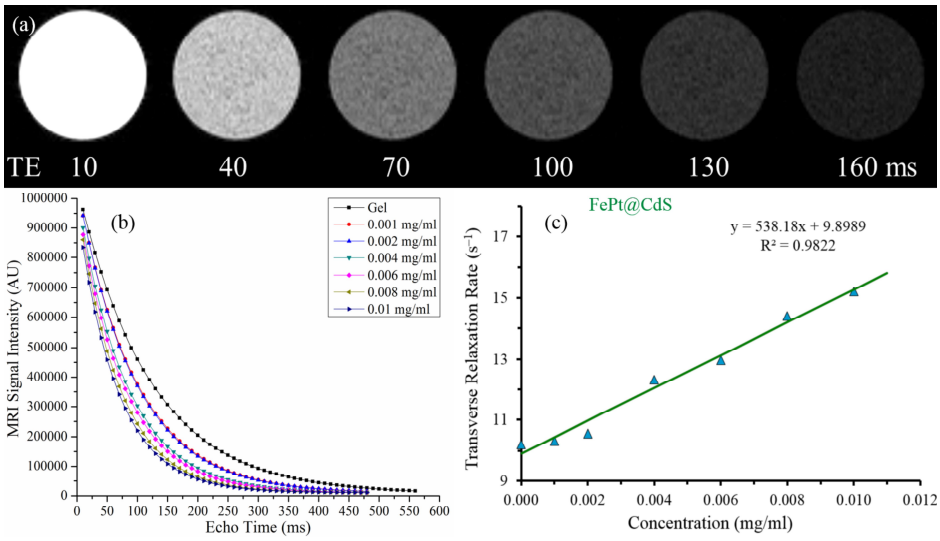

Figure 6.9 Transverse relaxivity characterization (a) typical MR images of microfuge tube containing FePt@CdS (0.01 mg/ml in 0.5% agarose gel), (b) estimation of transverse relaxation time (T_2) of water and (c) transverse relaxivity of FePt@CdS in 0.5% agarose gel

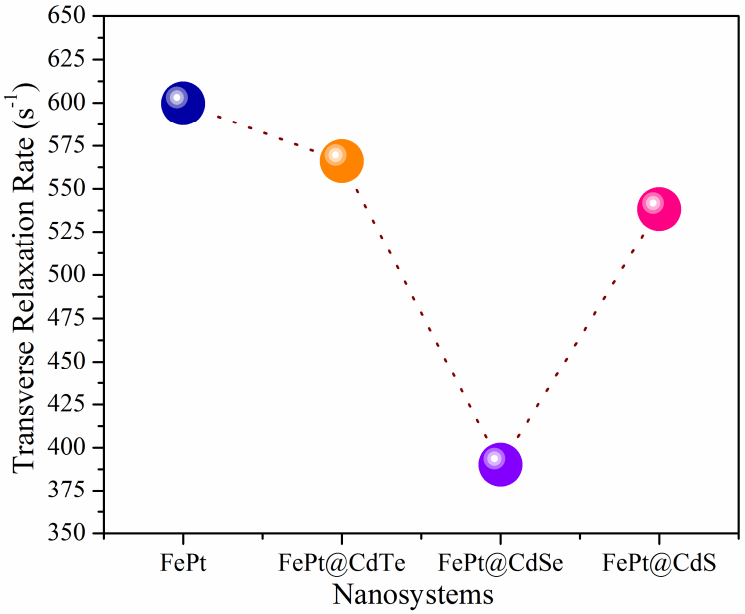

Figure 6.10 Comparative **t**ransverse relaxivity rate of pristine and hybrid nanosystems

The relaxivity (r_2), measure of the change in the spinï spin relaxation rate per unit concentration, is found to be 566.0, 390.1 and 538.1 s^{-1} mg^{-1} ml for the FePt@CdTe, FePt@CdSe and FePt@CdS hybrid nanosystems. The relaxivity (r_2) of the pristine FePt is 599.6 s^{-1} mg^{-1} ml which is shown in **figure 3.15(c)** in chapter 3. A comparative picture of transverse relaxivity rates of pristine and hybrid nanosystems are presented in **figure 6.10**. It is observed that there is a decrease in relaxivity of hybrid nanosystems as compared to the pristine FePt which is due to the nonmagnetic coating. Among all the hybrid nanosystems, FePt@CdSe has showed the lowest value of relaxivity which may be due to the thicker nonmagnetic shell growth as revealed in HRTEM images. It is also observed that the transverse relaxivity of FePt and hybrid nanosystems are superior to that of functionalized iron oxide nanoparticles [22, 24]. It is worthwhile to mention that iron oxide nanoparticles are already in use as contrast probe in clinical practice.

6.3 Conclusion

The magneto-fluorescent hybrid nanosystems open up a new approach to multimodal biomedical applications because of their integrated functionality. The *in vitro* cytotoxicity of the GSH capped magneto-fluorescent hybrid nanosystems were carried

out using RAW 264.7 macrophage cell line confirming its high biocompatibility. The magnetic (MRI contrast) and fluorescent imaging property of all hybrids depicts it is suitable contain both the functionality. Unlike other reported hybrid systems, the transverse relaxivity and the fluorescence efficiency are not compromised as compared to the pristine magnetic nanosystems and QDs. The slightly decrease transverse relaxivity observed in hybrid nanosystems as compared to the pristine magnetic system is due to the nonmagnetic shell of hybrid nanosystem. On the other hand, the enhanced fluorescence efficiency of hybrid nanosystem can be due more passivation effect of CdS than that in pristine QD system. Overall, all the developed magneto-fluorescent hybrid nanosystems are suitable for both FI and MR imaging.

References:

[1] Wiesmüller, M. *et al.* Comparison of lesion detection and quantitation of tracer uptake between PET from a simultaneously acquiring whole-body PET/MR hybrid scanner and PET from PET/CT. *Eur. J. Nucl. Med. Mol. Imaging* **40** (1), 12--21, 2013.

[2] Martinez-Moller, A. *et al.* Workflow and Scan Protocol Considerations for Integrated Whole-Body PET/MRI in Oncology. *Journal of Nuclear Medicine* **53** (9), 1415--1426, 2012.

[3] Drzezga, A. *et al.* First Clinical Experience with Integrated Whole-Body PET/MR: Comparison to PET/CT in Patients with Oncologic Diagnoses. *Journal of Nuclear Medicine* **53** (6), 845--855, 2012.

[4] Basu, S. *et al.* Quantitative Techniques in PET-CT Imaging. *Current Medical Imaging Reviews* **7** (3), 216--233, 2011.

[5] Hofmann, M. *et al.* MRI-based attenuation correction for PET/MRI: a novel approach combining pattern recognition and atlas registration. *J. Nucl. Med.* **49** (11), 1875--1883, 2008.

[6] Thorek, D. L. J. *et al.* Quantitative imaging of disease signatures through radioactive decay signal conversion. *Nat. Med.* **19** (10), 1345--1350, 2013.

[7] Daisne, J. F. *et al.* Evaluation of a multimodality image (CT, MRI and PET) coregistration procedure on phantom and head and neck cancer patients:

Accuracy, reproducibility and consistency. *Radiother. Oncol.* **69** (3), 237--245, 2003.

[8] Zarb, F. *et al.* Developing optimized CT scan protocols: Phantom measurements of image quality. *Radiography* **17** (2), 109--114, 2011.

[9] Plewes, D. B. & Kucharczyk, W. Physics of MRI: A primer. *Journal of Magnetic Resonance Imaging* **35** (5), 1038--1054, 2012.

[10] Keereman, V. *et al.* MRI-based attenuation correction for PET/MRI using ultrashort echo time sequences. *J. Nucl. Med.* **51** (5), 812--818, 2010.

[11] Abeylath, S. C. *et al.* Combinatorial-designed multifunctional polymeric nanosystems for tumor-targeted therapeutic delivery. *Acc. Chem. Res.* **44** (10), 1009--1017, 2011.

[12] Suh, W. H. *et al.* Multifunctional nanosystems at the interface of physical and life sciences. *Nano Today* **4** (1), 27--36, 2009.

[13] Chen, H. *et al.* A pH-responsive cyclodextrin-based hybrid nanosystem as a nonviral vector for gene delivery. *Biomaterials* **34** (16), 4159--4172, 2013.

[14] Motornov, M. *et al.* An Integrated multifunctional nanosystem from command nanoparticles and enzymes. *Small* **5** (7), 817--820, 2009.

[15] Chen, C. *et al.* Highly crystalline multimetallic nanoframes with three-dimensional electrocatalytic surfaces. *Science* **343** (6177), 1339--1343, 2014.

[16] Walzl, A. *et al.* The Resazurin Reduction Assay Can Distinguish Cytotoxic from Cytostatic Compounds in Spheroid Screening Assays. *J. Biomol. Screen.* **19** (7), 1047--1059, 2014.

[17] Xiao, J. *et al.* Monitoring of cell viability and proliferation in hydrogel-encapsulated system by resazurin assay. *Appl. Biochem. Biotechnol.* **162** (7), 1996--2007, 2010.

[18] Park, J. H. *et al.* Micellar hybrid nanoparticles for simultaneous magnetofluorescent imaging and drug delivery. *Angew. Chemie - Int. Ed.* **47** (38), 7284--7288, 2008.

[19] Chen, O. *et al.* Magneto-fluorescent core-shell supernanoparticles. *Nat. Commun.* **5**, 5093--5600, 2014.

[20] Thomas, R. *et al.* Magnetic iron oxide nanoparticles for multimodal imaging and therapy of cancer. *Int. J. Mol. Sci.* **14** (8), 15910--15930, 2013.

[21] Stephen, Z. R. *et al.* Magnetite nanoparticles for medical MR imaging. *Materials Today* **14** (7), 330--338, 2011.

[22] Bhattacharya, S. *et al.* Effect of biomimetic templates on the magneto-structural properties of Fe_3O_4 nanoparticles. *RSC Adv.* **5** (5), 13777--13786, 2015.

[23] Jha, D. K. *et al.* Direct synthesis of water dispersible superparamagnetic TGA capped FePt nanoparticles: One pot, one shot. *Mater. Chem. Phys.* **156**, 247--253, 2015.

[24] Bhattacharya, S. *et al.* Protein-polymer functionalized aqueous ferrofluids showing high T2 relaxivity. *J. Biomed. Nanotechnol.* **10** (5), 811--819, 2014.